Int. J. Electrochem. Sci., 7 **(2012)** 345 - 353

International Journal of
ELECTROCHEMICAL
SCIENCE
www.electrochemsci.org

Electrochemical Impedance Spectroscopy (EIS) Study of $LiNi_{1/3}Co_{1/3}Mn_{1/3}O_2$ for Li-ion Batteries

Li Wang, Jishi Zhao, Xiangming He[*], *Jian Gao, Jianjun Li, Chunrong Wan, Changyin Jiang*

Institute of Nuclear and New Energy Technology, Beijing Key Lab of Fine Ceramics, Tsinghua University, Beijing 100084, PR China
[*]E-mail: hexm@tsinghua.edu.cn

Received: 29 October 2011 / *Accepted:* 8 December 2011 / *Published:* 1 January 2012

Electrochemical impedance spectroscopy (EIS) is employed to investigate the electrochemical properties of $LiNi_{1/3}Co_{1/3}Mn_{1/3}O_2$ cathode. The Nyquist plots at initial state, 40%SOC, 80%SOC and 100%SOC at first cycle, second cycle and 10^{th} cycle, respectively, are investigated. The information of electrolyte resistance, surface film resistance and charge transfer resistance are obtained by modeling with two different equivalent circuits according with the Nyquist plots with different shape. The comparison between $LiCoO_2$ and $LiNi_{1/3}Co_{1/3}Mn_{1/3}O_2$ is also investigated in this study. It can be speculated that both the passivating film on the surface of $LiNi_{1/3}Co_{1/3}Mn_{1/3}O_2$ cathode and the channels for lithium ion transfer in $LiNi_{1/3}Co_{1/3}Mn_{1/3}O_2$ cathode are mostly formed during the first charge/discharge process. Both diffusion coefficient of lithium ion in $LiNi_{1/3}Co_{1/3}Mn_{1/3}O_2$ cathode and exchange current density are in accord with the analysis of the Nyquist plots of electrochemical impedance spectra, indicating the rationality of the speculation.

Keywords: Electrochemical impedance spectroscopy; kinetic properties; $LiNi_{1/3}Co_{1/3}Mn_{1/3}O_2$; Lithium-ion batteries

1. INTRODUCTION

In recent years, many researchers have applied electrochemical impedance spectroscopy (EIS) to study the kinetics of promising electrode materials for rechargeable lithium batteries [1-2]. Among these materials such as $LiFePO_4$ [3-4], $LiCoO_2$ [4-5] and $LiMn_2O_4$ [6-7] have been characterized extensively because of their high reversibility in Li-ion intercalation/de-intercalation processes.

So far, most of studies were carried out on composite electrodes [8-10] and thin-film electrodes [11-12], a single particle of micrometer size electrodes were also investigated with the aim of clarifying its electronic and ionic transport properties [13]. Results deduced with composite electrodes

are influenced by not only the electrochemical properties of the active materials but also the fabrication (*i.e.* organic binder, conductive additives, and porosity.) It is important to know the kinetic properties of lithium transport in the oxide host to determine the cycling performance, so, the stability of oxide during the charge/discharge process is desirable to be studied to enhance the performance of lithium ion batteries.

Electrochemical impedance spectroscopy (EIS) technique has been used to study the electrode materials because it can reveal the relationship between the crystal lattice with the electrochemical properties [14-15]. In this work, we report the electrochemical investigations on $LiNi_{1/3}Co_{1/3}Mn_{1/3}O_2$ cathode by EIS technique. Particularly, we demonstrate here that impedance of $LiNi_{1/3}Co_{1/3}Mn_{1/3}O_2$ cathode changed with cycles increasing, which help us to know the influence of the impedance of electrode on its cycling performance. Both the apparent chemical diffusion coefficient of lithium ion (D_{Li^+}) in $LiNi_{1/3}Co_{1/3}Mn_{1/3}O_2$ cathode and the exchange current density (j_0) are obtained from the analysis of impedance spectra. The comparison of EIS analysis between $LiCoO_2$ and $LiNi_{1/3}Co_{1/3}Mn_{1/3}O_2$ are also presented.

2. EXPERIMENTAL

In this study, the $LiNi_{1/3}Co_{1/3}Mn_{1/3}O_2$ particles are prepared based on controlled crystallization and solid state reaction. And the particles are spherical; the results of X-ray Diffraction show that there is no impurity in the particles accord with the JCDS standard. Moreover, the size distribution of particles is between 7um and 12um. This is different from the previous work. For electrochemical performance evaluation, half-cell studies are performed.

The $LiNi_{1/3}Co_{1/3}Mn_{1/3}O_2$ powder is mixed with acetylene black and PTFE dissolved in ethanol in the weight ratio of 8:1:1 to form slurry. After solvent evaporation, the electrode is pressed and dried at 120^{o}C under vacuum over 24 h. CR2025-type coin cells are assembled in a glove box (M. Braun GmbH, Germany) with H_2O and O_2 content below 1 ppm. Metallic lithium foil is used as counter electrode. The electrolyte is 1.0 M $LiPF_6$ dissolved in a mixture of ethylene carbonate (EC), ethyl methyl carbonate (EMC) and dimethyl carbonate (DMC) (1:1:1, v/v) and Celgard 2400 polyethylene is used as the separator.

EIS is done using the ZAHNER-IM6eX electrochemical workstation (Germany) at room temperature. The EIS measurements are performed with 10 mV perturbation amplitude in the range from 100 kHz to 5 mHz in automatic sweep mode from high to low frequencies. The impedance spectra are recorded at each state allowing at least 5 additional hours for equilibration after each charging/discharging step.

The counter electrode is lithium foil about 1.0 cm^2 and the electrochemical measurements are performed with a two-electrode system. The counter electrode is large enough, so it almost does not affect the EIS behavior. Data acquisition and analysis are done, respectively, using the electrochemical impedance software.

3. RESULTS AND DISCUSSION

3.1. Analysis of the electrochemical impedance spectra

Fig. 1 displays the -Nyquist plots of the EIS obtained from the $LiNi_{1/3}Co_{1/3}Mn_{1/3}O_2$ cathode at the different state at first, second and 10th cycle charge/discharge process, respectively.

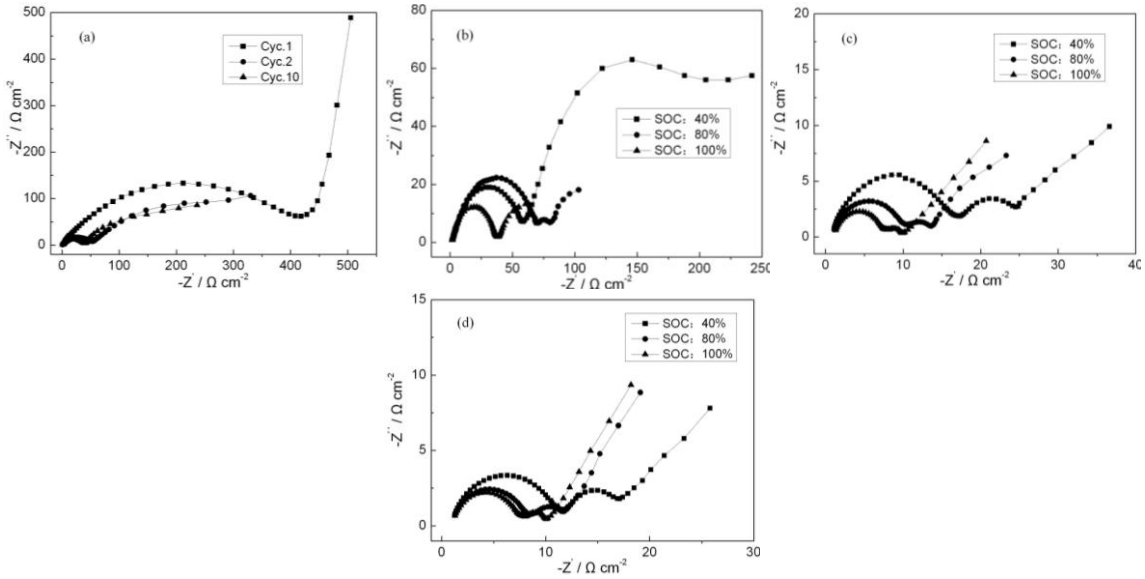

Figure 1. Nyquist plots of $LiNi_{1/3}Co_{1/3}Mn_{1/3}O_2$ cathode. (a) the plots at the initial state (0% SOC) of first, second and 10th cycle; (b) the plots at 40%SOC, 80%SOC and 100%SOC of first cycle; (c) the plots at 40%SOC, 80%SOC and 100%SOC of second cycle; (d) the plots at 40%SOC, 80%SOC and 100%SOC of 10th cycle.

As shown in Fig. 1(a), the -Nyquist plots consist of an out-of-shaped semicircle alike in appearance of a half ellipse in high and intermediate frequency ranges and a straight line inclined at a constant angle to the real axis in the lower frequency range at the initial state. However, the Nyquist plots at 0% SOC are different from each other at the first, second and 10th cycle. The difference takes places in the lower frequency range. To compare with that at first cycle, the semicircles at the second and 10th cycles are much smaller.

Moreover, another effect to be noticed is the large difference in impedance response between Fig.1(a) and Fig.1(b, c, d). This difference is basically in the lowest frequency semicircle of the dispersion, which shows an increasing tendency to close to the real axis ($Z^{'}$) as the voltage increases. Since the interface between the current collector and the $Li_{1-x}Ni_{1/3}Co_{1/3}Mn_{1/3}O_2$ cathode is blocking for lithium ions, the imaginary part of Z ($Z^{''}$) would tend to be infinity as the frequency tends to zero. The fact that the semicircle however tends to close to the real axis ($Z^{'}$) can reasonably be explained by the change of the electronic conductivity of $Li_{1-x}Ni_{1/3}Co_{1/3}Mn_{1/3}O_2$ with x. Indeed, this assumption is supported by some literatures, which demonstrates that the material passes from an insulator when x is

close to unity, to a conductor when x assumes lower value [16-19]. By the way, the analysis for the impedance spectra will be done to explain this phenomenon in the latter section.

Also, it can be found that the semicircles appeared in the high frequency range show no obvious changes with the SOC increasing from 80% to 100%, which reveals that the passivating film is stable. The radius of the semicircle appeared in moderate frequency range decrease with the voltage increasing, revealing that the decreasing of the charge-transfer resistance. One reason applied to explain the phenomena is that the ionic conductivity of the cathode materials increases with the SOC increasing.

Fig. 1(b, c, d) display the electrochemical impedance spectra of the $LiNi_{1/3}Co_{1/3}Mn_{1/3}O_2$ cathode in different cycles at initial state, 40% SOC, 80% SOC and full charged state, respectively. It is found that the shape of the -Nyquist plots are alike for different cycles after the first cycle. That is, the -Nyquist plots for the initial state at different cycle consist of one semicircle at high frequency range and a line at lower frequency range; and the -Nyquist plots at 40% SOC, 80% SOC and full charged consist of two anomalous semicircles with compressed shape in high and moderate frequency range and a anomalous line at lower frequency range. Also, the radius of the semicircle decrease with the cycle increasing. Moreover, the difference in radius between the first cycle and the second circle is larger than that between the second cycle and the tenth cycle, revealing that the passivating film forms mostly during the first charge/discharge process and is stable during the latter charge/discharge cycles. Obviously, comparing with the increasing cycle, the state of charge (SOC) has much more influence on the impedance after the first charge/discharge cycle.

Table1. Nyquist Analysis of LiNi1/3Co1/3Mn1/3O2/Li coin cell (Ω cm-2)

parameter	SOC / Cycle	0%SOC	40%SOC	80%SOC	100%SOC
Re	cyc.1	1.69	0.99	2.04	1.44
	cyc.2	0.63	0.71	0.92	0.77
	cyc.10	0.84	0.81	0.86	0.91
Rct	cyc.1	372.9	63.38	62.11	5.83
	cyc.2	241.41	9.58	7.74	3.73
	cyc.10	201.82	6.11	3.08	2.18
Rsf	cyc.1	*	104.63	50.95	32.13
	cyc.2	47.75	15.36	11.34	9.09
	cyc.10	38.05	10.43	7.38	6.56

In order to investigate the changes in the EIS spectra of $LiNi_{1/3}Co_{1/3}Mn_{1/3}O_2$ electrode during the charging process in detail, we employed equivalent circuits displayed in Fig. 2 to analyze the impedance spectra data shown in Table 1. For the $LiNi_{1/3}Co_{1/3}Mn_{1/3}O_2$ cathode at the initial state in the 10^{th} cycle (with 0% SOC), typically one dispersed semicircle within the frequency range (100K Hz-44.1 Hz) is observed. The total impedance could be regarded as the electrolyte resistance R_e and the charge transfer resistance R_{ct}, and C_{dl} is the double-layer capacitance. Z_w is the Warburg impedance

that reflects the diffusion of lithium-ion in the solid. C_L means simply the intercalation capacitance. As shown in Fig.2, when $LiNi_{1/3}Co_{1/3}Mn_{1/3}O_2$ electrode is charged at 0.1C rate to 40% SOC, the shape of the impedance spectra changes totally and two semicircles are observed. In other words, the semicircle at high-frequency range (100K Hz-55.9 Hz) and the semicircle at lower frequency range (55.9 Hz-0.33 Hz) are separated.

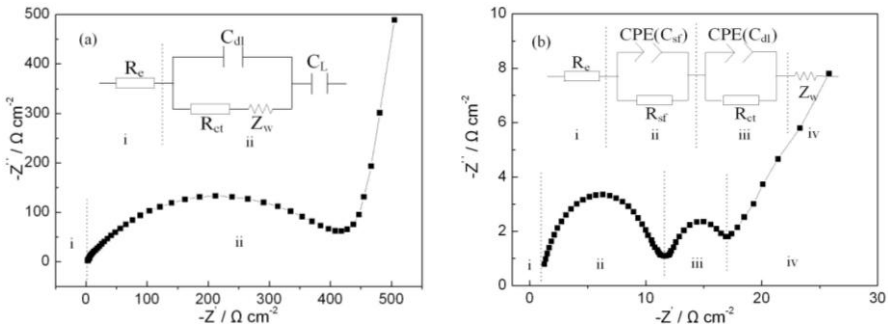

Figure 2. EIS plots and their equivalent circuits of $LiNi_{1/3}Co_{1/3}Mn_{1/3}O_2$ cathode. (a) for 0%SOC;(b) for 40%SOC, 80%SOC and 100%SOC.

The semicircle at high frequency can be ascribed to the electrolyte resistance and the surface film impedance (represented by $R_e(R_{sf} \| CPE(C_{sf}))$), and the semicircle at lower frequency can be ascribed to the lithium-intercalation process (represented by $R_{ct} \| CPE(C_{dl})$), the approximate beeline closed to the second semicircle (in the frequency range of 0.33 Hz-0.005 Hz) reveals the diffusion of lithium-ion in the $LiNi_{1/3}Co_{1/3}Mn_{1/3}O_2$ cathode, which can be represented by Z_w series to the others parts in the equivalent circuit given in the insert of Fig. 2(a). It should be mentioned that the constant phase element (*CPE*) has been introduced in equivalent circuit (b) instead of pure capacitive element C_{sf} and C_{dl} . Though the equivalent circuit simulated by the electrochemical impedance software is different from the previous research [14-15], it can match the measurement results totally. In others cycles, the shape of the impedance spectra and their equivalent circuit are the same as that shown in Fig. 2(b). The fitting results, including R_e, R_{sf} and R_{ct}, are summarized in Table 1.

Table 1 displays the variation of R_e, R_{sf} and R_{ct} with potential, respectively. It can be found that R_e at initial state (with 0% SOC) decreases after the first cycle, revealing that the charge/discharge process enhance the transference performance of lithium-ion in the electrolyte. R_e decreases with SOC increasing in the first cycle, and there is no obvious differences at the same cycle with different SOC after the first cycle. The relationship between R_{sf} and the SOC in different charge/discharge cycles in Table 1 reveals that R_{sf} at the first charge/discharge process with 40% SOC is much larger than that of others. In the first charge/discharge process, R_{sf} decreases sharply from 104.63 $\Omega\ cm^{-2}$ to 50.95 $\Omega\ cm^{-2}$ with the SOC increases from 40% to 80%. The SOC has strong influence on R_{sf} in the all cycles. It is speculated that the passivating surface film of the cathode is mainly formed during the forepart in the first charge/discharge process, and then keeps stable in the subsequent cycles. Moreover, the contact performance between electrolyte and cathode electrode at the beginning of the charging process should

be also considered, which has been proposed by Holzapfel et al. [20] during the research on the first lithiation and charge/discharge cycles of graphite materials. Fortunately, the analysis results of R_{sf} is in accord with the inferences. As shown in Table 1, the trend of charge transfer resistance R_{ct} *vs* SOC is the same with that of R_{sf} *vs* SOC.

3.2. Diffusion coefficient and exchange current density

The exchange current density and the lithium ion diffusion coefficient can be calculated according to the following equation, respectively:

$$j_0 = \frac{i_0}{A} = \frac{RT}{nFR_{ct}A} \quad (1)$$

$$D_{Li^+} = R^2T^2 / 2A^2n^4F^4C^2\sigma^2 \quad (2)$$

where j_0 and D_{Li^+} are the exchange current density and the diffusion coefficient of lithium ion, respectively. R means the gas constant, T is the absolute temperature (the number is 298.15 in present work), and n is the number of electrons per molecule during oxidization (n =1 according to the reaction of lithium ion intercalation/de-intercalation), F is the Faraday's constant, A is the area of the cathode/electrolyte interface, it is 0.5 cm^{-2} in this work. The value of R_{ct} is deduced from the modeling of EIS data discussed above. C *is* the concentration of lithium ion, and σ is the Warburg factor which has relationship with Z_{re} ($\omega = 2\pi f$):

$$Z_{re} = R_D + R_L + \sigma\omega^{1/2} \quad (3)$$

The relationship between $-Z_{re}$ and square root of frequency ($\omega^{-1/2}$) in low frequency region are shown in Fig. 3 as follows:

The diffusion coefficient of lithium ion (D_{Li^+}) calculated based on equations (2) and (3) [21] is displayed in Table 2. D_{Li^+} increases with the SOC increasing from 0% to 80% in every charge/discharge process, and also increases with the increasing cycles at a given SOC. It also can be found that the difference between the first cycle and the second cycle is more evident than that between the second cycle and the tenth cycle. Croce et al. [22] has proved that the de-intercalation of lithium-ion from the oxide cathode materials reduces the de-intercalation of lithium-ion from oxide cathode material de-shields the electrostatic repulsion between the oxygen of two adjacent layers and expands the crystal lattice, resulting in improving the diffusion properties of lithium-ion in oxide cathode materials. Combination with the results shown in Table 1, it can be speculated that such processes is mostly occurred during the first cycle. The exchange current density (j_0) calculated by equation (1) [13] is also shown in Table 2. Absolutely, comparing with D_{Li^+}, j_0 is influenced by SOC and cycles in the same way. The calculated results indicate that the rationality of the supposition that

both the passivating film of $LiNi_{1/3}Co_{1/3}Mn_{1/3}O_2$ cathode and the channels for lithium-ion transference in $LiNi_{1/3}Co_{1/3}Mn_{1/3}O_2$ cathode are mainly formed during the first charge/discharge process.

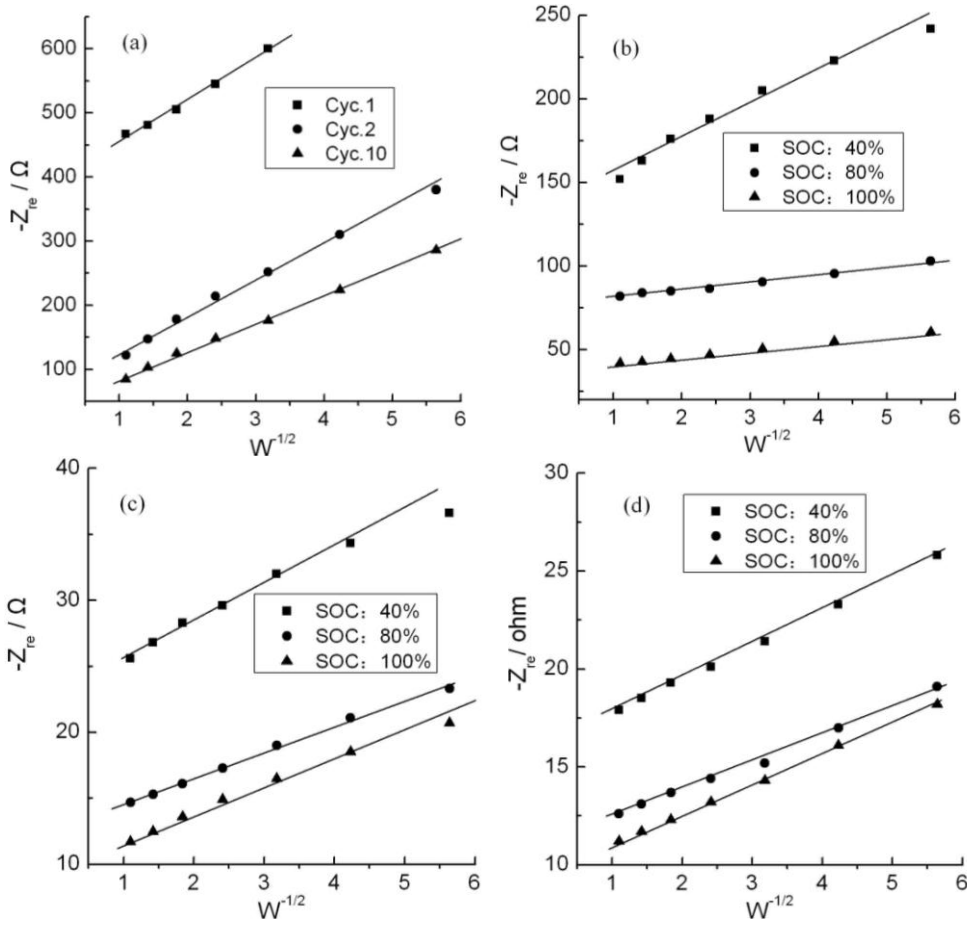

Figure 3. the relationship between $-Z_{re}$ and $\omega^{-1/2}$ at low frequency region (*a*: the initial state at different cycles; *b*: first cycle at different SOC; *c*: Second cycle at different SOC; *d*: 10th at different SCO)

Table 2. The diffusion coefficient of lithium-ion (D_{Li^+}) in cathode and exchange current density (j_0) at different state of charge

Parameters / State	D_{Li^+} / cm^2 S^{-1}			j_0 /A cm^2		
	First cycle	Second cycle	Tenth cycle	First cycle	Second cycle	Tenth cycle
0% SOC	3.86E-17	4.71E-17	9.14E-17	1.38E-04	2.13E-04	2.55E-04
40% SOC	1.72E-16	2.91E-14	7.29E-14	8.11E-04	0.00536	0.00842
80% SOC	2.01E-14	1.04E-13	1.98E-13	8.27E-04	0.00664	0.01668
100% SOC	3.53E-14	1.22E-13	2.41E-13	0.00881	0.01377	0.02357

3.3. Comparison between $LiNi_{1/3}Co_{1/3}Mn_{1/3}O_2$ and $LiCoO_2$

Table 3 shows the R_e, R_{sf}, R_{ct}, D_{Li^+} and j_0 of $LiNi_{1/3}Co_{1/3}Mn_{1/3}O_2$ and $LiCoO_2$ [23] at different SOC of 10th cycle.

Table 3. Nyquist Analysis of LiNi1/3Co1/3Mn1/3O2 and LiCoO2 cathode at tenth cycle

parameter	SOC	$LiNi_{1/3}Co_{1/3}Mn_{1/3}O_2$	$LiCoO_2$
R_e/Ω cm^{-2}	0%	0.84	2.03
	40%	0.81	1.22
	80%	0.86	1.19
	100%	0.91	1.09
R_{sf}/Ω cm^{-2}	0%	38.05	11.31
	40%	10.43	6.6
	80%	7.38	4.80
	100%	6.56	4.58
R_{ct}/Ω cm^{-2}	0%	201.82	16.31
	40%	6.11	20.44
	80%	3.08	10.34
	100%	2.18	8.30
D_{Li^+} / cm^2 S^{-1}	0%	9.14E-17	2.11E-16
	40%	7.29E-14	1.42E-13
	80%	1.98E-13	1.42E-12
	100%	2.41E-13	1.25E-12
j_0 /A cm^{-2}	0%	2.55E-04	0.00315
	40%	0.00842	0.00251
	80%	0.0167	0.00497
	100%	0.0236	0.00619

The values of R_e for both of $LiNi_{1/3}Co_{1/3}Mn_{1/3}O_2$ and $LiCoO_2$ at different SOC of 10th cycle are small. That for $LiCoO_2$ is slightly bigger. The R_{sf} can make sense to understand the materials, which for $LiNi_{1/3}Co_{1/3}Mn_{1/3}O_2$ is much bigger. That for $LiCoO_2$ changes a little at different SOC%, indicating the better stability of $LiCoO_2$ electrode than $LiNi_{1/3}Co_{1/3}Mn_{1/3}O_2$ electrode. The R_{ct} indicates the electronic conductivity of the materials. EIS analysis shows that the $LiNi_{1/3}Co_{1/3}Mn_{1/3}O_2$ material has quite big value of R_{ct} at the beginning of charge process, indicating the low electronic conductivity. However, The R_{ct} of $LiNi_{1/3}Co_{1/3}Mn_{1/3}O_2$ cathode decrease rapidly from 201.82 Ω cm^{-2} to 6.11 Ω cm^{-2} after charge process, afterwards the value keeps stable. D_{Li^+} and j_0 indicate the ion diffusion and reversibility of electrochemical reaction. This study shows that D_{Li^+} of $LiCoO_2$ is bigger than that for $LiNi_{1/3}Co_{1/3}Mn_{1/3}O_2$; and j_0 of $LiNi_{1/3}Co_{1/3}Mn_{1/3}O_2$ is bigger than that for $LiCoO_2$, indicating the difference between these two materials for their electrochemical performance. This analysis indicates the direction of modification on these materials.

4. CONCLUSION

In attempts to investigate the kinetics properties of $LiNi_{1/3}Co_{1/3}Mn_{1/3}O_2$ cathode, EIS technique has been employed to try to understand more about this material. The analysis has shown that the R_{sf} is

the most important factor to control the kinetics properties of $LiNi_{1/3}Co_{1/3}Mn_{1/3}O_2$ cathode. The calculated results indicate that the rationality of the supposition that both the passivating film of $LiNi_{1/3}Co_{1/3}Mn_{1/3}O_2$ cathode and the channels for lithium-ion transference in $LiNi_{1/3}Co_{1/3}Mn_{1/3}O_2$ cathode are mainly formed during the first charge/discharge process. This study shows that D_{Li^+} of $LiCoO_2$ is bigger than that for $LiNi_{1/3}Co_{1/3}Mn_{1/3}O_2$; and j_0 of $LiNi_{1/3}Co_{1/3}Mn_{1/3}O_2$ is bigger than that for $LiCoO_2$, indicating the difference between these two materials for their electrochemical performance. This analysis indicates the direction of modification on these materials.

ACKNOWLEDGEMENT

This work is supported by the Ministry of Science and Technology (Grant No. 2011CB935902 and Grant No. 2010DFA72760), the National Natural Science Foundation of China (Grand No.20901046 and Grand No.20903061) and the Tsinghua University Initiative Scientific Research Program (Grand No. 2010THZ08116).

References

1. K. M. Shaju, G. V. S. Rao, B. V. R. Chowdari. *Electrochimica Acta*. 48 (2003) 2671.
2. S. Q. Liu, S. C. Li, K. L. Huang, B. L. Gong, G. Zhang. *J. Alloys Compd*. 450 (2008) 499.
3. F. Gao, Z. Y. Tang. *Electrochimica Acta*. 53 (2008) 5071.
4. J. X. Ma, C. S. Wang, S. Wroblewski. *J. Power Sources* 164 (2007) 849.
5. H. W. Yan, X. J. Huang, H. Li, L. Q. Chen. *Solid State Ionics* 113-115 (1998):11.
6. R. Yazami, Y. Ozawa. *J. Power Sources* 153 (2006) 251.
7. A.K. Hjelm, G. Lindbergh. *Electrochim. Acta*. 47 (2002) 1747.
8. G. M. S. R. Thomas, P. G. Bruce, J. B. Goodenough. *J. Electrochem. Soc*. 132 (1985) 1521.
9. G. M. S. R. Thomas, P. G. Bruce, J. B. Goodenough. *Solid State Ionics* 18-19 (1986) 794.
10. M. D. Levi, G. Salitra, B. Markovsky, H. Teller, D. Aurbach, U. Heider, L. Heider. *J. Electrochem. Soc*. 146 (1999) 1279.
11. J. M. McGraw, C. S. Bahn, P. A. Parilla, J. D. Perkins, D. W. Readey, D. S. Ginley. *Electrochim. Acta*. 45 (1999)187.
12. H. Sato, D. Takahashi, T. Nishina, I. Uchida. *J. Power Sources* 68 (1997)540.
13. K. Dokko, M. Mohamedi, Y. Fujita. *J. Electrochem. Soc*. 148 (2001) A422.
14. J. P. Meyers, M. Doyle, R. M. Darling, J. Newman. *J. Electrochem. Soc*. 147(2000) 2930.
15. J. Euler, W. Nonnenmacher. *Electrochim. Acta*. 2 (1960) 268.
16. F. Croce, A. Deptula, W. Lada, R. Marassi, T. Olczak, F. Ronci. *Ionics* 3 (1997) 390.
17. M. D. Levi, G. Salitra, B. Marcowsky, H. Teller, D. Aurbach, U.Heider, L. Heider. *J. Electrochem. Soc*. 146 (1999) 1279.
18. J. Molenda, A. Stopklosa, T. Bak. *Solid State Ionics* 36 (1989) 53.
19. M. Shibuya, T. Nishina, T. Matsue, I. Uchida. *J. Electrochem. Soc*. 143 (1996) 3157.
20. M. Holzapfel, A. Martinent, F. Alloin, B. LeGorrec, R. Yazami, C. Montella. *J. Electroanal. Chem*. 546 (2003) 41.
21. H. Liu , C. Li , H. P. Zhang, L. J. Fu, Y. P. Wu, H. Q. Wu. *J. Power Sources* 159 (2006) 717.
22. F. Croce, F. Nobili, A. Deptula, W. Lada, R. Tossici, A. D'Epifanio, B. Scrosati, R. Marassi. *Electrochem. Commun*. 1 (1999) 605.
23. J.S. Zhao, L. Wang, X.M. He, C.R. Wan, C.Y. Jiang, *Int. J. Electrochem. Sci*. 2010 ,5(4): 478-488